INVITED PAPER

FORMATION OF THE NANOCRYSTALLINE CUBIC (FeNi)$_{23}$B$_6$ PHASE IN THE NICKEL-RICH FeNiZrB ALLOYS AND ITS MAGNETIC BEHAVIOUR

B. Idzikowski[*], A. Szajek

Institute of Molecular Physics, Polish Academy of Sciences, M. Smoluchowskiego 17
PL 60-179 Poznán, Poland

Nickel-rich amorphous precursor with nominal chemical composition of Ni$_{64}$Fe$_{16}$Zr$_7$B$_{12}$Au$_1$ was produced by melt-spinning technique and then heat-treated at temperatures ranged from 420 to 465°C for one hour, to form nanostructure. The transformation from the amorphous state into the nanocrystalline state was investigated by DSC and XRD techniques. Due to annealing in amorphous matrix appear grain fraction (5-50 nm in diameter) of magnetically ordered cubic Fe$_x$Ni$_{23-x}$B$_6$ phase, as was identified by XRD measurements. The magnetic behaviour of pure Ni$_{23}$B$_6$ and Fe$_{23}$B$_6$ phases was studied theoretically using the spin polarized tight binding linear muffin-tin orbital (*TB-LMTO*) method. Anomalously high magnetic moments of Fe atoms were found in some nonequivalent positions in the crystal structure.

1. Introduction

Soft nanocrystalline alloys prepared by controlled heat treatment of amorphous precursors are interesting because of their magnetic properties specially combined with high permeability. Ultrafine grain structure of the order of few or several nanometres embedded in residual amorphous matrix is responsible for magnetic behaviour of the alloy. In literature are described various techniques used for structural and magnetic investigations in order to understand such kind of two-phase magnetic system.

The nanocrystalline magnetic materials are among the key materials supporting next generation of electronic devices. Up to now these alloys, produced by partial crystallization of amorphous precursors, exhibit a two- or more-phase structure with body centred cubic (bcc) nanocrystalline grains dispersed in the residual amorphous matrix. All known soft magnetic nanocrystalline alloys consist of nanosized bcc-Fe(Si) [1], bcc-Fe [2] or bcc-(FeCo) [3] grains with 3-15 nm in diameter. During the devitrification processes the amorphous part of alloys becomes inhomogeneous showing sometimes significant gradients of compositions.

Due to the magnetic exchange interactions, nanocrystalline systems consisting of soft magnetic phase placed in an amorphous matrix can reveal a smooth magnetization curve near zero field with extremely small coercive force. In these materials, also, remanence B$_r$ value close to saturation J$_s$ values can be observed. Values B$_r$/J$_s$ larger than 0.5 are very often ascribed to an exchange coupling between grains of soft magnetic phase, but they can also be due to the anisotropy of the soft phase obeying cubic symmetry. Obviously, in both cases the assumptions of non-interacting particles with an isotropic distribution of magnetically easy axes leading to the Stoner-Wohlfarth value B$_r$/J$_s$ = 0.5 are violated. The coercive force values for non coupled system are described by Alben equations [4] and discussed in the frame of random anisotropy model (RAM) by Harris, Plischke and Zuckermann [5]. But, finally, Herzer [6] explained the phenomena of magnetic softening in nanocrystalline materials.

---

[*] Corresponding author: idzi@ifmpan.poznan.pl

The magnetic properties as well as the crystallization behaviour of Ni-containing amorphous alloys were studied earlier but those alloys were unsuitable to form the nanocrystalline phase or phases. Presence of such elements like Nb, Zr, Mo, Ti in the precursor alloy is needed to block the grain growth. The extremely fine nanocrystalline structure is expected if in the amorphous precursor are present clusters of e.g. Cu or Au. So far exists only $Fe_{40}Ni_{38}Mo_4B_{18}$ system in which the nano-structured phase was found by the XRD method [7,8]. Presence in the alloy of Mo atoms plays a crucial role in the process of nanostructure formation.

It is of particular interest to study such alloys and to attempt to understand the details of the complex crystallization process leading to the formation of fcc-based soft magnetic nanostructured systems. For this purpose we prepared a novel nickel-rich amorphous alloy in which the nanostructure is possible to form, as usually, by controlled annealing but the significant presence of Ni in this alloy results in the formation of metastable nickel-rich fcc-phase containing both of transition elements (Ni and/or Fe) and boron.

2. Experimental

Melt-spun alloys with the nominal composition $Ni_{64}Fe_{16}Zr_7B_{12}Au_1$ were prepared by the single roller (40 cm in diameter) technique in Ar protective atmosphere. High-purity elements (Ni 99.995, Fe 99.998, B 99.8, Zr 99.95%, Au 99.995) were used to make starting prealloys. Each ingot was several times turned over and melted in a furnace heated by induction. Water cooled boat was used to ensure homogeneity. The dimensions of the obtained long ribbons are 3 mm wide and 0.35 μm thick. The structure of the samples was characterized by X-ray diffraction analysis in a Seifert diffractometer using $Cu-K_\alpha$ radiation. The crystallization behaviour of as-quenched ribbons was examined by differential scanning calorimetry using a DSC 404 apparatus produced by Netzsch. The TEM samples were prepared by argon ion milling using 10 keV Ar^+ ions. TEM investigation was done on a Philips CM20 microscope, (TWIN configuration, accelerating voltage: 200 kV), equipped with a Noran Voyager EDS system with Ge(Li) detector.

3. Results of measurements

Crystallization of amorphous $Ni_{64}Fe_{16}Zr_7B_{12}Au$ alloys, as investigated by DSC linear-heting curves, clearly shows two crystallization stages with two characteristic crystallization temperatures. Such a behaviour is typical for amorphous alloys serving as the precursors for the formation of the nanocrystalline alloys [9]. The crystallization temperature of the first stage is about 460 °C. DSC measurement, not shown here, was carried out with 20 K/min heating rate.
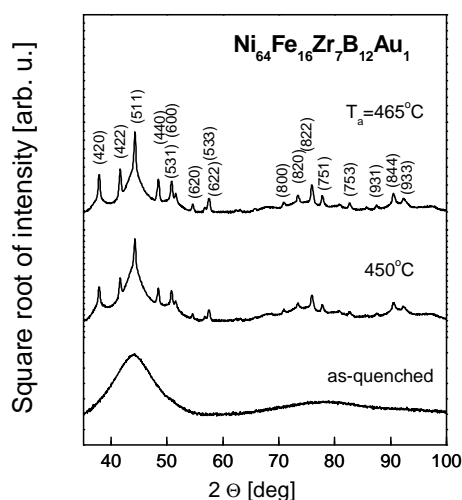

Fig. 1. XRD patterns for as-quenched $Ni_{64}Fe_{16}Zr_7B_{12}Au_1$ ribbon and after annealing at 450 °C and 465 °C for one hour.

Fig. 1 shows the structure of Ni$_{64}$Fe$_{16}$Zr$_7$B$_{12}$Au$_1$ amorphous alloy and partially crystallized after annealing at temperatures 450°C and 465°C for one hour. The as-quenched sample is fully amorphous with a broad peak around 43° (2θ). As a result of the annealing in amorphous matrix there appear grains (5-50 nm in diameter) of magnetically ordered cubic Fe$_x$Ni$_{23-x}$B$_6$ phase. All peaks are identified and these belong to the C$_6$Cr$_{23}$-type structure described by space group Fm$\overline{3}$m. TEM picture for this heat treated sample is shown in Fig. 2. Fraction of very small grains (several nanometers in diameter) is present among big grains. The annealed nanocrystalline ribbons became magnetically soft because of the exchange interaction between these small grains.
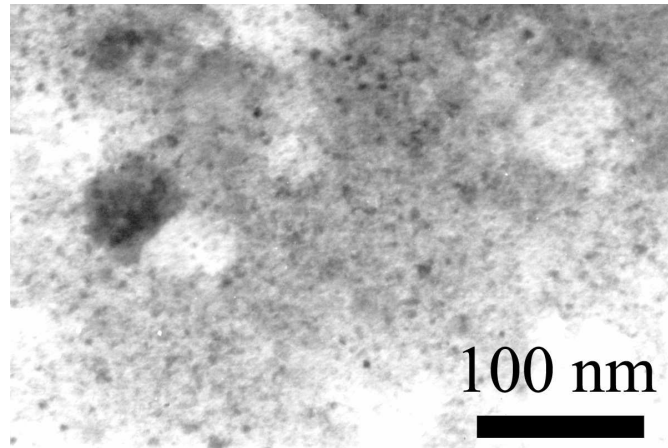
Fig. 2. TEM micrograph for Ni$_{64}$Fe$_{16}$Zr$_7$B$_{12}$Au$_1$ annealed at 465°C for one hour.

4. Details of band structure calculations

The spin polarized tight binding linear muffin-tin orbital (*TB-LMTO*) method in the atomic sphere approximation (*ASA*) [10,11] was used to compute the electronic band structure of Fe$_{23}$B$_6$ and Ni$_{23}$B$_6$ compounds. In this approximation, the crystal is divided into space-filling spheres, therefore with slightly overlapping spheres centred on each of the atomic sites. The standard combined corrections for overlapping [10] were employed to compensate *ASA* errors. In the calculations reported here, the Wigner-Seitz (*WS*) sphere radii are such that the overlap is equal to 9.792% and 9.993% for Fe$_{23}$B$_6$ and Ni$_{23}$B$_6$, respectively. The total volumes of all spheres S_j (j=1, …, N) are equal to the equilibrium volume (V) of the unit cell with the experimental value of lattice constant of Fe$_{23}$B$_6$ [12] (for Ni$_{23}$B$_6$ compound we assumed the same value): $V=(4\pi/3)\Sigma_j S_j^3=(4\pi/3)N(S_{av})^3$, where S$_{av}$ is average *WS* radius. The systems are cubic (Fm$\overline{3}$m space group no. 225); their unit cells accommodate four formula units with N=116 atoms. There are four inequivalent positions of Fe (Ni) atoms (see Table 1).

Table 1. Structural parameters of Fe$_{23}$B$_6$ and Ni$_{23}$B$_6$ (a=10.761Å [12], S$_{av}$=1.36879 Å) and *WS* radii S_j[Å].

Atom (position)		x	y	z	S_j	
					Fe$_{23}$B$_6$	Ni$_{23}$B$_6$
Fe or Ni	(4a)	0	0	0	1.7007	1.7236
Fe or Ni	(8c)	¼	¼	¼	1.5576	1.5799
Fe or Ni	(48h)	0	0.1699	0.1699	1.3852	1.3757
Fe or Ni	(32f)	0.3809	0.3809	0.3809	1.3543	1.3447
B	(24e)	0.2765	0	0	1.1908	1.2115

As starting, the atomic configurations were assumed: core[Ar] + $3d^6 4s^2$ for Fe, core [He] + $2p^2 2s$ for B, and core[Ar] + $3d^8 4s^2$ for Ni. The fully relativistic approach for the core electrons and scalar relativistic approximation for the valence electrons were used. The Min-Jang [13] scheme for calculating the spin-orbit effects was employed. The exchange-correlation potential was chosen in the form proposed by von Barth-Hedin [14]. The selfconsistent calculations were performed for 256 k-points in the irreducible wedge (1/48) of the Brillouin zone. The tetrahedron method [15] was used for integration over Brillouin zone. The iterations were repeated until accuracy of the energy eigenvalues within the error of 0.01 mRyd was achieved.
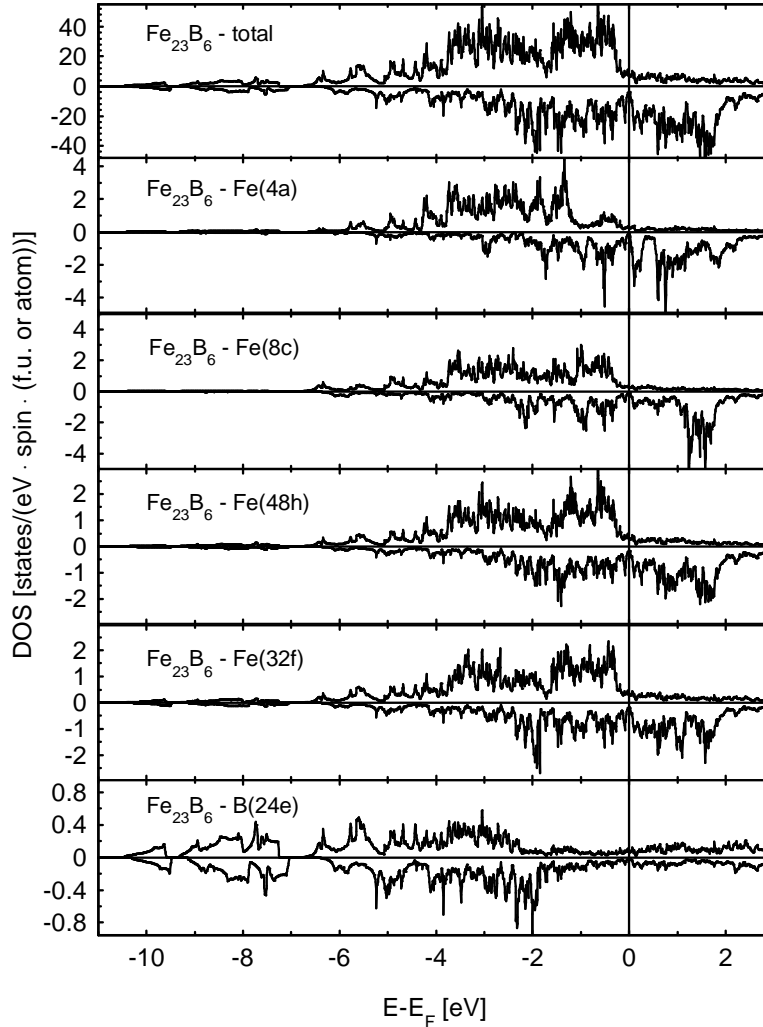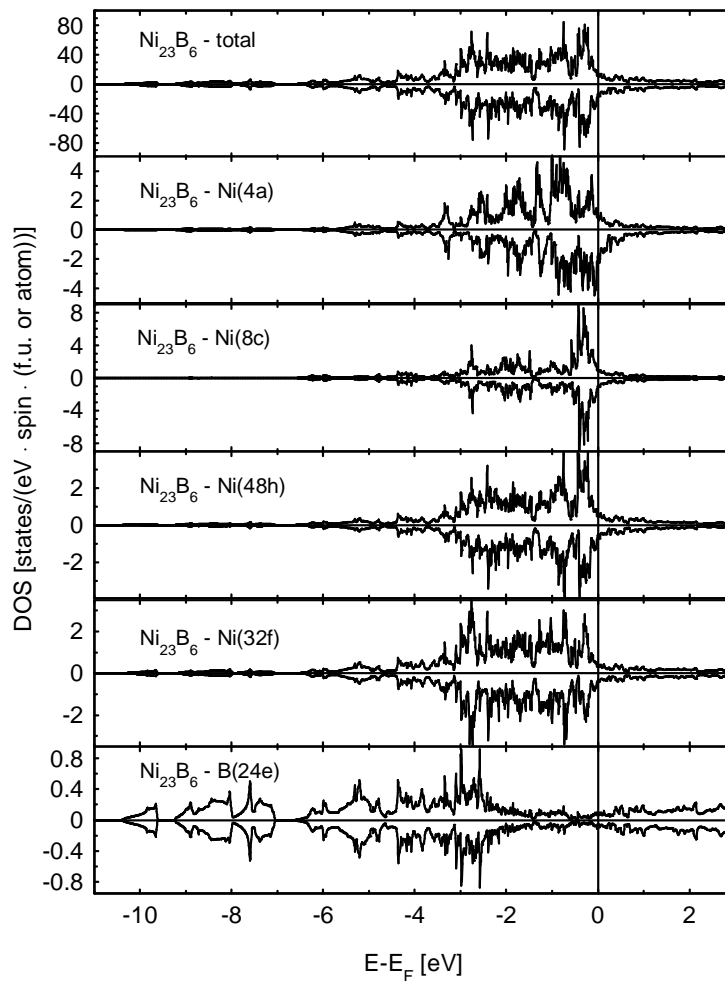

Fig. 3. Total and local DOS plots for $Fe_{23}B_6$ compound.

5. Results of calculations

The total and local densities of states (DOS) are presented in Fig. 3 and 4 for $Fe_{23}B_6$ and $Ni_{23}B_6$ compounds, respectively. The shape of DOS plots depends on the type of atom, its localization and local environment. The values of total DOS at the Fermi level (E_F) are equal to 10.589 and 25.184 states/(eV·f.u.) for $Fe_{23}B_6$ and $Ni_{23}B_6$ compounds, respectively. Because of large number of d electrons, that type of electrons provides the main contribution to the total DOS for $E=E_F$: about 90%. The exact values of site and l-decomposed spin-projected DOS at the Fermi level are collected in Table 2.

Table 2. DOS at the Fermi level [states/(eV·spin·(atom or f.u.)].

Atom (position)	Site and spin projected DOS (per atom)		Type of DOS	Total and l-decomposed spin projected DOS (per f.u.)	
	spin ↑	spin ↓		spin ↑	spin ↓
Fe$_{23}$B$_6$:			Total	6.577	4.012
Fe (4a)	0.227	0.140			
Fe (8c)	0.239	0.104	Total for:		
Fe (48h)	0.270	0.176	s electrons	0.310	0.030
Fe (32f)	0.281	0.182	p electrons	0.923	0.147
B (24e)	0.064	0.016	d electrons	5.344	3.835
Ni$_{23}$B$_6$:			Total	11.857	13.327
Ni (4a)	0.801	1.765			
Ni (8c)	0.930	1.023	Total for:		
Ni (48h)	0.520	0.536	s electrons	0.364	0.300
Ni (32f)	0.317	0.345	p electrons	0.923	0.733
B (24e)	0.070	0.054	d electrons	10.570	12.294

Fig. 4. Total and local DOS plots for Ni$_{23}$B$_6$ compound.

The calculated total magnetic moments for $Fe_{23}B_6$ and $Ni_{23}B_6$ compounds are equal to 48.758 and 0.742 μ_B/f.u.. Local contributions provided by particular atoms are collected in Table 3.

Table 3. Local magnetic moments for Fe, Ni, and B atoms in $Fe_{23}B_6$ and $Ni_{23}B_6$ compounds.

Compound	Magnetic moments [μ_B/atom] for given position				
	4a	8c	48h	32f	24e
$Fe_{23}B_6$	2.982	2.553	2.222	1.877	-0.167
$Ni_{23}B_6$	0.347	0.015	0.032	-0.001	-0.002

Especially high values of magnetic moments are located on Fe(4a) and Fe(8c) atoms, higher than for bulk bcc-Fe system (about 2.2 μ_B/atom). The values of the magnetic moments depend on local environment of Fe atoms. Increasing number of neighbouring boron atoms reduces the magnetic moment of iron. In the case of $Ni_{23}B_6$ compound the magnetic moments are reduced (fcc-Ni: about 0.6 μ_B/atom): for Ni(4a) atom the magnetic moment is equal to 0.34 μ_B/atom, and for other sites the values are close to zero.

6. Conclusions

Band structure calculations showed that the local magnetic moments of Fe and Ni atoms in $Fe_{23}B_6$ and $Ni_{23}B_6$ compounds depend on their local environments. The iron magnetic moments are enhanced up to about 3 μ_B/atom and for nickel reduced, down to zero. The presented investigations will be continued for $(Fe_{1-x}Ni_x)_{23}B_6$ systems to establish dependence of magnetization on concentration of Ni impurities and the site preference of Ni.

After annealing, ribbons became extremely magnetically soft and in a nanocrystalline state show also good mechanical properties, as compared with the FINEMET, NANOPERM or HITPERM. The improved magnetic properties and reduced brittleness of the samples offer attractive possibilities for applications of this novel Ni-rich alloy.

References

[1] Y. Yoshizawa, S. Oguma, K. Yamauchi, J. Appl. Phys. **64**, 6044 (1988).
[2] K. Suzuki, N. Ktaoka, A. Inoue, A. Makino, T. Masumoto, Mat. Trans. JIM **31**, 743 (1990).
[3] M. A. Willard, D. E. Laughlin, M. E. McHenry, D. Thoma, K. Sickafus, J. O. Cross, V. G. Harris, J. Appl. Phys. **84**, 6773 (1998).
[4] R. Alben, J. J. Becker, M. Chi, J. Appl. Phys. **49**, 1653 (1978).
[5] R. Harris, M. Plischke, M. J. Zuckermann, Phys. Rev. Lett. **31**, 160 (1973).
[6] G. Herzer, Phys. Scripta. **T49**, 307 (1993).
[7] K. P. Mizgalski, O. T. Inal, F. G. Yost, M. M. Karnowsky, J. Mater. Sci. **16**, 3357 (1981).
[8] J. Li, Z. Su, T. M.Wang, S. H. Ge, H. Hahn, Y. Shiari, J. Mater. Sci. **34**, 111 (1999).
[9] J. W. Kondoro, S. J. Campbell, Hyperfine Inter. **55**, 993 (1990).
[10] O. K. Andersen, O. Jepsen, M. Šob, Electronic Structure and Its Applications, edited by M. Yussouff, Springer, Berlin (1987), p.2
[11] G. Krier, O. Jepsen, A. Burkhardt, O. K. Andersen, The TB-LMTO-ASA Program (source code, version 4.7).
[12] Y. Khan, H. Wibbeke, Z. Metalkd. **82**, 703 (1991).
[13] B. I. Min, Y.-R. Jang, J. Phys.: Condens. Matter **3**, 5131 (1991).
[14] U. von Barth, L. Hedin, J. Phys. **C 5**, 1629 (1972).
[15] P. Blöchl, O. Jepsen, O. K. Andersen, Phys. Rev. **B 49**, 16223 (1994).